



HAL
open science

Seismic hazard in western Canada from GPS strain rates versus earthquake catalog

Stephane Mazzotti, L. J. Leonard, J. F. Cassidy, G. C. Rogers, S. Halchuk

► **To cite this version:**

Stephane Mazzotti, L. J. Leonard, J. F. Cassidy, G. C. Rogers, S. Halchuk. Seismic hazard in western Canada from GPS strain rates versus earthquake catalog. *Journal of Geophysical Research*, 2011, 116, pp.B12310. 10.1029/2011JB008213 . hal-00689004

HAL Id: hal-00689004

<https://hal.science/hal-00689004>

Submitted on 30 Apr 2021

HAL is a multi-disciplinary open access archive for the deposit and dissemination of scientific research documents, whether they are published or not. The documents may come from teaching and research institutions in France or abroad, or from public or private research centers.

L'archive ouverte pluridisciplinaire **HAL**, est destinée au dépôt et à la diffusion de documents scientifiques de niveau recherche, publiés ou non, émanant des établissements d'enseignement et de recherche français ou étrangers, des laboratoires publics ou privés.

Seismic hazard in western Canada from GPS strain rates versus earthquake catalog

S. Mazzotti,^{1,2,3} L. J. Leonard,¹ J. F. Cassidy,^{1,2} G. C. Rogers,^{1,2} and S. Halchuk⁴

Received 16 January 2011; revised 10 September 2011; accepted 1 October 2011; published 17 December 2011.

[1] Probabilistic seismic hazard analyses (PSHA) are commonly based on frequency - magnitude statistics from 50–100 yearlong earthquake catalogs, assuming that these statistics are representative of the longer-term frequency of large earthquakes. We test an alternative PSHA approach in continental western Canada, including adjacent areas of northwestern U.S.A., using regional strain rates derived from 179 Global Positioning System (GPS) horizontal velocities. GPS strain rates are converted to earthquake statistics, seismic moment rates, and ground shaking probabilities in seismic source zones using a logic-tree method for uncertainty propagation. Median GPS-based moment rates and shaking estimates agree well with those derived from earthquake catalogs in only two zones (Puget Sound and mid-Vancouver Island). In most other zones, median GPS-based moment rates are 6–150 times larger than those derived from earthquake catalogs (shaking estimates 2–5 times larger), although the GPS-based and catalog estimates commonly agree within their 67% uncertainties. This discrepancy may represent an under-sampling of long-term moment rates and shaking by earthquake catalogs in some zones; however a systematic under-sampling is unlikely over our entire study area. Although not demonstrated with a high confidence level, long-term regional aseismic deformation may account for a significant part of the GPS/catalog discrepancy and, in some areas, represent as much as 90% of the total deformation budget. In order to integrate GPS strain rates in PSHA models, seismic versus aseismic partitioning of long-term deformation needs to be quantified and understood in terms of the underlying mechanical processes.

Citation: Mazzotti, S., L. J. Leonard, J. F. Cassidy, G. C. Rogers, and S. Halchuk (2011), Seismic hazard in western Canada from GPS strain rates versus earthquake catalog, *J. Geophys. Res.*, 116, B12310, doi:10.1029/2011JB008213.

1. Introduction

[2] Probabilistic seismic hazard analysis (PSHA) is one of the most common methods used to estimate ground shaking probabilities for engineering and public safety applications [e.g., *Earthquake Engineering Research Institute Committee on Earthquake Risk*, 1989; *U.S. National Research Council*, 1988]. This method typically relies on statistics of earthquake return period versus magnitude that are derived from a catalog of instrumental, historical, and paleoseismic data. Except in a few regions such as California, Japan, or New Zealand, historical and paleoseismic data availability remain limited, and 50–100 yearlong instrumental catalogs are the most common source of data used to derive earthquake statistics. The underlying assumption of this approach is that

statistics over 50–100 years are adequate to derive return periods over timescales of 500–5000 years typically used in PSHA. Obvious limitations are that earthquake occurrences and statistics may not be steady state over timescales of hundreds of years, and that a 100-year sample may not capture enough events to represent a robust statistical estimate.

[3] Owing to improvements of geodetic techniques in the last two decades, there have been numerous attempts to compare geodetic and seismic estimates of crustal strain rates and to use geodetic strain rates as a constraint on seismic moment rates and earthquake statistics for PSHA [e.g., *Working Group on California Earthquake Probabilities (WGCEP)*, 1995]. Despite the variety of methods, the outcomes typically fall into one of two categories: (1) agreement, within the data uncertainties, between geodetic and seismic rates [e.g., *Field et al.*, 1999; *Mazzotti et al.*, 2005], or (2) geodetic rates significantly larger than seismic ones [e.g., *Ward*, 1998a, 1998b; *Masson et al.*, 2005]. The latter cases are commonly explained in terms of either aseismic crustal deformation or under-sampling of the short earthquake catalog (compared to steady state/long-term rates). These potential under-sampling limitations of earthquake catalogs and biases in earthquake statistics raise the issue of under-estimation of the long-term seismic hazard.

¹Geological Survey of Canada, Natural Resources Canada, Sidney, British Columbia, Canada.

²Also at School of Earth and Ocean Sciences, University of Victoria, Victoria, British Columbia, Canada.

³Now at Geosciences Montpellier, UMR 5243, Université Montpellier 2, Montpellier, France.

⁴Geological Survey of Canada, Natural Resources Canada, Ottawa, Ontario, Canada.

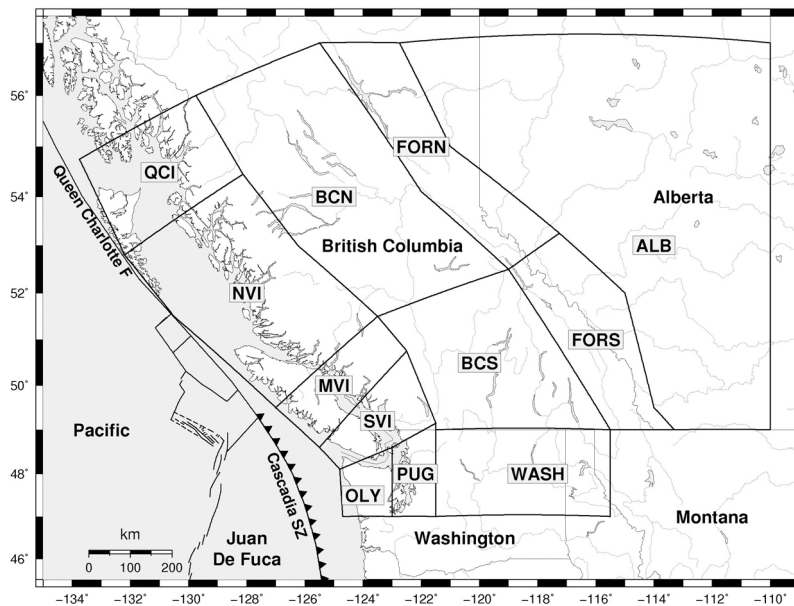


Figure 1. Western Canada–northwestern U.S.A. source zones. Thick solid lines show seismic source zones, with acronyms (cf. Table 1). Queen Charlotte F: Queen Charlotte Fault. Cascadia SZ: Cascadia Subduction Zone.

[4] In this paper, we present a detailed comparison of strain rates, seismic moment rates, and ground shaking probabilities derived from earthquake catalog and from Global Positioning System (GPS) data in western Canada and northwestern U.S.A. (Figure 1), focusing on continental crust seismicity. Our study area covers about $1500 \times 1000 \text{ km}^2$ and is divided into twelve seismic source zones on the basis of tectonic, geological and geodetic considerations. The seismic zone settings vary from low-strain intraplate regions (Alberta), to the mid-strain Cordillera (central British Columbia), to high-strain plate boundary regions (western British Columbia, northern Washington). The variety of geodynamic settings and strain rates allows us to test if the agreements or differences between earthquake catalog and geodetic rates can be related to parameters such as strain rate amplitude, regional tectonics, or plate-boundary seismic cycle.

[5] The comparison of ground shaking probabilities derived from the earthquake catalog and from GPS data provides a basis for testing the feasibility of using GPS strain rates as a constraint for PSHA. Using our results, we discuss some of the limitations and requirements to allow the integration of GPS strain rates in PSHA.

2. Data and Method

2.1. Tectonic and Geodynamic Background

[6] Our study area ranges from stable intraplate North America to the active Pacific–North America and Juan de Fuca–North America plate boundaries (Figure 1). To the east, the Alberta plains are characterized by a relatively cold geotherm and strong lithosphere rheology, as shown by numerous indicators such as surface heat flow, mantle shear wave velocity, and effective elastic thickness. In contrast,

the same proxies indicate that the Cordillera is associated with a hot geotherm and weak lithosphere rheology [e.g., *Hyndman et al.*, 2005]. As a result of this lithospheric strength contrast, the Alberta plains have been part of stable North America since $\sim 1.5 \text{ Ga}$, whereas the Cordillera has acted as a plate-boundary zone accommodating the relative motion between the North America plate to the east and various oceanic plates to the west for the last $\sim 150 \text{ Ma}$.

[7] Present-day tectonics also reflect this contrast. The Alberta plains are characterized by low tectonic strain rates and low-level seismicity (Figure 2). To the west, the 40–50 mm/yr relative plate motion is primarily accommodated along two major plate-boundary faults: the Cascadia subduction fault and the Queen Charlotte transform fault (Figure 1). About 10–20% of this relative motion is transferred landward and accommodated by internal deformation of the Cordilleran lithosphere [*Mazzotti et al.*, 2008]. However, this pattern is strongly heterogeneous along the strike of the plate boundary zone, with variations of a factor of ~ 10 in the amount of seismicity and crustal strain between very active regions and very quiescent regions (e.g., Puget Sound versus north-central BC, Figure 2).

2.2. Catalog Earthquake Statistics and Seismic Moment Rates

[8] We divide the study area in twelve seismic source zones (Figure 1) within which we estimate earthquake catalog statistics and moment rates. The zone geometries are chosen to maximize the following criteria: homogeneous spatial and temporal seismicity distribution; consistent tectonic and stress patterns; consistent GPS strain rate style (and amplitude). We use the Geological Survey of Canada earthquake catalog (Figure 2), which extends to northern

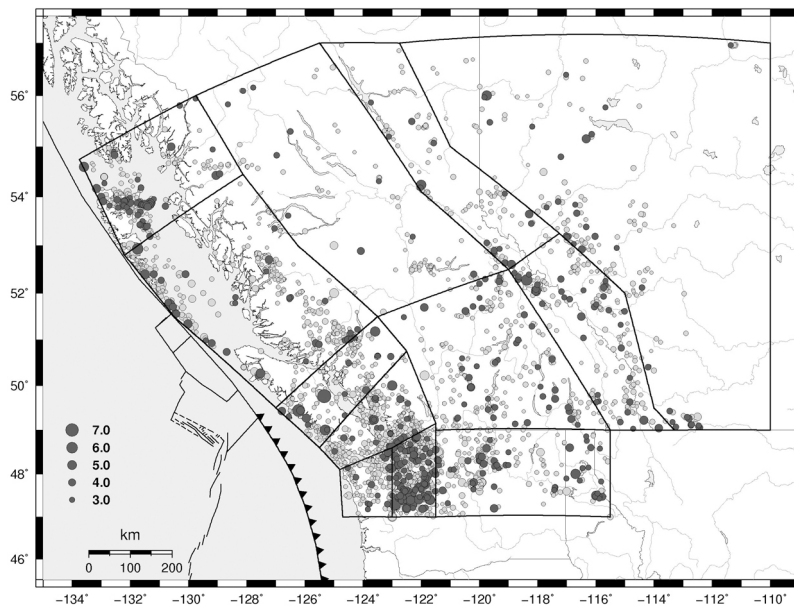


Figure 2. Earthquakes and seismic source zones. Continental crustal earthquakes from GSC catalog, magnitude $M \geq 2.0$, 1899–2009 (light gray circles). Dark gray circles show earthquakes $M \geq 3.0$ that pass completeness test. Earthquakes occurring in the oceanic plates, along the Queen Charlotte and Cascadia plate-boundary faults (Figure 1), and induced earthquakes are omitted.

Washington and Montana and provides a consistent set of earthquake locations, times and magnitudes that is the basis for the Canadian National Seismic Hazard Model. Our analysis focuses on crustal (upper plate) deformation and seismic hazard. Thus, we remove induced earthquakes related to oil and gas production in the Rocky Mountain Foothills, as well as offshore earthquakes along the main plate boundary faults and in the oceanic plates in the coastal zones of the Queen Charlotte and Cascadia margins. We do not decluster the catalog as it does not show any clear case of aftershock sequences following the very few $M_W \geq 6$ earthquakes.

[9] Within each seismic zone, we use a maximum likelihood inversion [Weichert, 1980] to calculate the a and b

parameters that best fit a cumulative exponential-truncated Gutenberg-Richter (GR) distribution:

$$\begin{aligned} N(m) &= 10^a e^{-b \ln(10)m} (1 - e^{-b \ln(10)(M_X - m)}) \rightarrow m < M_X \\ N(m) &= 0 \rightarrow m \geq M_X \end{aligned} \quad (1)$$

where $N(m)$ is the cumulative number of earthquakes of magnitude m and larger, M_X is the maximum magnitude, a is the seismicity level, and b is the slope of the GR distribution (Table 1). The maximum likelihood method of Weichert [1980] uses different completeness periods for different magnitude ranges, thus allowing the integration of large earthquakes back to about 1900–1920 in most of our study area. For each seismic zone, the magnitude -

Table 1. Earthquake Catalog Statistics and Moment Rates^a

Zone	Location	N	M_X	b		a		\dot{M}_0^S			$\dot{M}_0^C / \dot{M}_0^S$, Med
				Med	σ	Med	σ	Med (10^{17} Nm yr ⁻¹)	Min (10^{17} Nm yr ⁻¹)	Max (10^{17} Nm yr ⁻¹)	
QCI	Queen Charlotte Islands	68	7.5	0.83	0.09	2.75	0.26	1.02	0.25	4.12	0.05
NVI	North Vancouver Island– South Queen Charlotte	36	7.5	0.68	0.10	1.99	0.28	1.72	0.37	8.05	0.10
FORN	Foreland Belt–North	15	7.0	0.70	0.16	1.63	0.48	0.23	0.02	2.58	0.11
FORS	Foreland Belt–South	40	7.0	0.85	0.12	2.52	0.36	0.23	0.04	1.42	0.56
ALB	Alberta Plains	35	7.0	1.18	0.18	3.47	0.54	0.03	>0.01	0.36	0.85
BCN	Central BC–North	11	7.0	1.76	0.49	4.73	1.44	>0.01	>0.01	1.62	5.93
BCS	Central BC–South	42	7.0	0.96	0.13	2.80	0.39	0.10	0.01	0.68	0.04
MVI	Mid Vancouver Island	16	7.5	0.41	0.10	0.69	0.29	3.95	0.86	18.10	2.28
WASH	Northeast Washington	51	7.0	0.88	0.11	2.64	0.32	0.20	0.04	0.99	0.16
SVI	South Vancouver Island	37	7.5	0.82	0.11	2.33	0.33	0.50	0.08	3.02	0.31
PUG	Puget Lowland	112	7.5	0.77	0.06	2.66	0.18	2.15	0.81	5.70	0.33
OLY	Olympic Mountains	18	7.5	0.82	0.16	2.04	0.48	0.23	0.02	3.12	0.12

^aZone: source zone abbreviation (Figure 1). N: number of earthquakes used in catalog magnitude-frequency fit. M_X : median value of the maximum magnitude of the GR distribution (equation (1) and Table 2). b and a: best fit slope and intercept of cumulative truncated magnitude-frequency distribution (equation (1)). \dot{M}_0^S : statistical seismic moment rate (equation (2)). $\dot{M}_0^C / \dot{M}_0^S$: ratio of summation to statistical moment rate; Parameters are presented as a median (med) and 67% confidence interval, either as a standard error (σ) or a lower and upper bound (min, max).

Table 2. Seismic Moment Logic-Tree Parameters^a

Param.	Low.	Med.	Upp.	Prob.	Zones
μ (N m ²)	2.3×10^{10}	3.0×10^{10}	3.7×10^{10}	0.275/0.45/0.275	All
h (km)	10	20	30	0.3/0.4/0.3	QCI, NVI, FORN, FORLS
h (km)	20	25	30	0.3/0.4/0.3	ALB, MVI, SVI, PUG, OLY
h (km)	10	12	15	0.3/0.4/0.3	BCN, BCS, WASH
$\dot{\epsilon}^G$ (yr ⁻¹)	cf. Table 3	cf. Table 3	cf. Table 3	0.275/0.45/0.275	All
φ	1.06	1.27	1.71	0.275/0.45/0.275	All
b	cf. Table 1	cf. Table 1	cf. Table 1	0.275/0.45/0.275	All
c/d	1.5/9.0	1.5/9.05	1.5/9.1	0.275/0.45/0.275	All
M_X	7.2	7.5	7.8	0.275/0.45/0.275	QCI, NVI, MVI, SVI, PUG, OLY
M_X	6.5	7.0	7.5	0.3/0.4/0.3	FORN, FORLS, ALB, BCN, BCS, WASH

^aParam.: Parameters used in the seismic moment rate calculations (equations (4) and (7)); μ : shear modulus; h : seismic thickness; $\dot{\epsilon}^G$: average scalar strain rate; φ : moment – magnitude asymmetry correction factor; b : slope of GR distribution (equation (1)); c/d : moment – magnitude parameters; M_X : maximum magnitude. Low., Med., Upp.: Lower, median, and upper values for individual parameters. Prob.: Probabilities associated with the lower, median, and upper values. Zones: Source zones in which the parameter range applies. Cf. Appendix A for details.

completeness tables are adapted from the Canadian National Seismic Hazard Model [Adams and Halchuk, 2003] and are based on the history of the seismograph network, type of instruments, and detection levels (see auxiliary material).¹

[10] The a and b values are primarily constrained by the small and mid-size earthquakes ($M \leq \sim 4.5$), and are not too sensitive to the choice of M_X , providing there are enough small earthquakes. In several zones, the number of earthquakes is relatively small (< 20) and can be regarded as a poor constraint, especially on the b value (Table 1). Thus, we consider an alternative analysis where the b value is fixed to the average for the whole catalog ($b = 0.8$) and only the a value is solved for (equation (1)). The results of this test, as well as other systematic uncertainty tests, are presented in Appendix C and discussed in sections 3 and 4.

[11] The seismic moment rate within each seismic zone can be calculated assuming that the GR distribution defines the long-term frequency statistics for each magnitude range. The statistical seismic moment rate \dot{M}_0^S is derived by integrating the cumulative truncated GR distribution up to the maximum magnitude M_X [Hyndman and Weichert, 1983]:

$$\dot{M}_0^S = \varphi \frac{b}{c-b} 10^{[(c-b)M_X + a + d]} \quad (2)$$

where φ is a correction for the asymmetry of the stochastic magnitude - moment relation ($\varphi = 1.27$ assuming a standard error of 0.2 on magnitudes [Hyndman and Weichert, 1983]), and c and d are the parameters of the magnitude (m) - moment (M_0) relation:

$$\log_{10}(M_0) = cm + d \quad (3)$$

For onshore western Canada, the catalog M_L magnitudes are similar to M_W magnitudes, with $c = 1.5$ and $d = 9.05$ [Ristau et al., 2005].

[12] We estimate the median value and 67% confidence interval of \dot{M}_0^S (Table 1) using a logic-tree method where each parameter (or parameter set) is represented by a lower, median, and upper value with associated probabilities. This method is commonly used in PSHA and was adapted for regional strain rate and seismicity analyses by Mazzotti and Adams [2005] and Mazzotti et al. [2005]. The choice of parameter ranges and probabilities is explained in Appendix A

¹Auxiliary materials are available in the HTML. doi:10.1029/2011JB008213.

and presented in Table 2. The maximum magnitude has a significant effect on the statistical moment rate; e.g., an increase of 1 magnitude unit results in an increase of the moment rate by a factor of ~ 5.4 (equation (2)). We use M_X values adapted from the most recent Canadian and U.S. National Seismic Hazard Maps [Adams and Halchuk, 2003; Petersen et al., 2008], with median $M_X = 7.0$ and $M_X = 7.5$ for the interior and plate-boundary source zones, respectively. As described in the U.S. and Canadian hazard models, these values are primarily based on the dimensions of known U.S. active faults and considerations of the maximum dimension of other mapped faults and structures ($< \sim 150$ km).

[13] Alternatively, the total moment rate in each seismic zone can be calculated by summing the moment of each earthquake in the catalog normalized by the appropriate return period [e.g., Ward, 1998a, 1998b]. Typically, moment rates derived from catalog summations are significantly smaller than those derived from statistical integration, due to the lack of large earthquakes in the instrumental catalog. This is the case for all but two of our seismic zones, where the ratio of summation to statistical moment rate is significantly less than one (Table 1). The other two zones (*MVI* and *BCN*) are characterized by a low number of earthquakes and relatively poor GR statistics.

2.3. GPS Data and Strain Rates

[14] The GPS data set used in this study is presented in Figure 3. It comprises 179 horizontal velocity vectors derived from 89 continuous and 90 campaign GPS stations throughout Alberta, British Columbia, and northern Washington [Henton et al., 2006; Leonard et al., 2007; Mazzotti et al., 2003a, 2003b] (see auxiliary material). Data time spans vary from 1992 to 2008, with an average time series length of 5–6 years. Details of the regional network processing are given in Mazzotti et al. [2003b] and Leonard et al. [2007]. The various networks are combined, aligned to the International Terrestrial Reference Frame ITRF2000, and referenced to stable North America using the North America/ITRF2000 rigid rotation [cf. Mazzotti et al., 2008].

[15] On the west coast, the GPS velocity field is strongly influenced by interseismic strain accumulation along the currently locked Cascadia subduction fault and Queen Charlotte transform fault. This interseismic strain is mainly elastic and will be almost entirely reversed during future large earthquakes along those faults. Thus, this component of the GPS velocity field has to be removed in order to

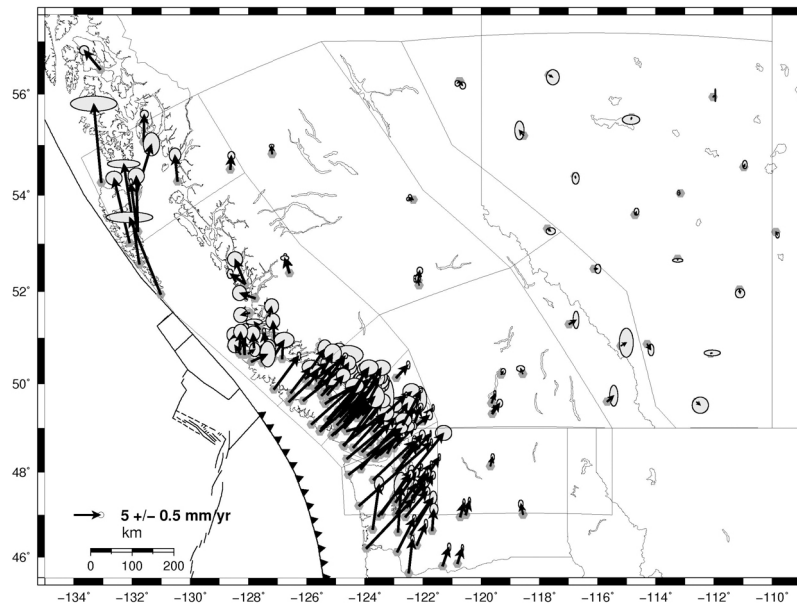


Figure 3. Horizontal GPS velocities. Black arrows show horizontal GPS velocities, relative to stable North America (in ITRF2000). Gray ellipses show 67% confidence intervals.

estimate the long-term tectonic strain of the Cordillera. We use the interseismic loading models developed for the Cascadia subduction zone [Wang *et al.*, 2003] and the Queen Charlotte transform and under-thrusting faults [Mazzotti *et al.*, 2003b] to correct the GPS velocities. Detailed descriptions of the applied corrections are given by Mazzotti *et al.* [2008].

[16] More recently, alternative interseismic models have been proposed for the northern Cascadia subduction zone

[McCaffrey *et al.*, 2007; Yoshioka *et al.*, 2005] and the Queen Charlotte margin [Elliott *et al.*, 2010; Hippchen and Mazzotti, 2010]. To first order, these studies confirm the strong interseismic locking of the Cascadia and Queen Charlotte Fault; however, they vary in the details of interseismic locking distribution and deformation. Our preferred interseismic model is based on uniform 100% locking, but we test two additional cases with a reduced interseismic locking of 75% and a steeper locking depth profile

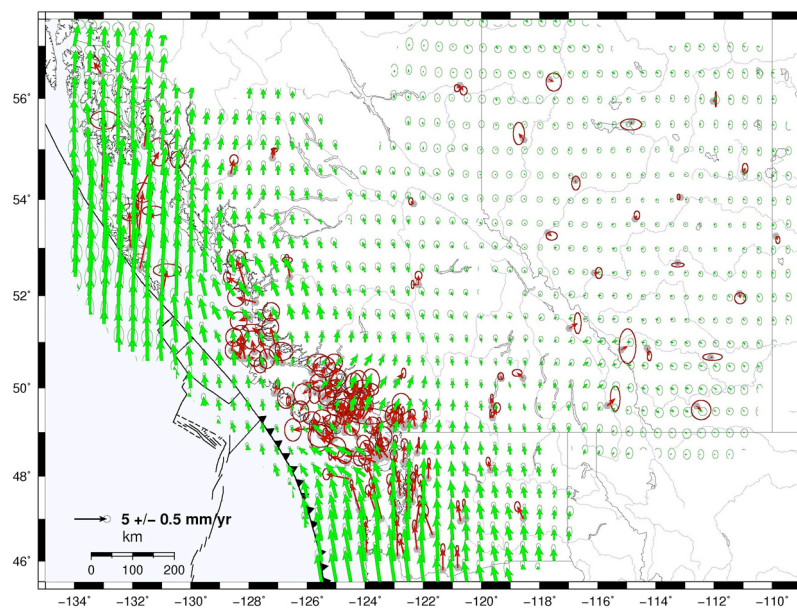


Figure 4. Smoothed residual GPS velocity field. Red arrows are residual GPS velocities (after correction for interseismic strain accumulation along plate-boundary faults: dip slip on Cascadia subduction fault; strike- and dip-slip on Queen Charlotte fault system; cf. text). Green arrows show interpolated smoothed velocity field on 0.5×0.5 degree grid. Ellipses show 67% confidence intervals. Interpolated values are masked in areas farther than 150 km from nearest GPS station.

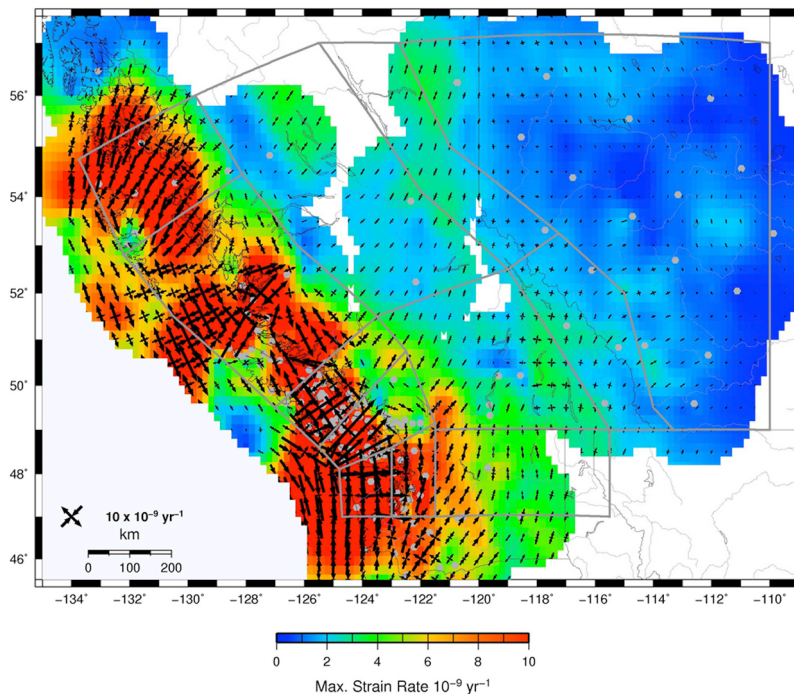


Figure 5. Smoothed residual GPS strain rate field. Black arrows show the interpolated smoothed strain rate tensors on 0.5×0.5 degree grid. Color background map shows scalar maximum strain rate (cf. text). Interpolated values are masked in areas farther than 150 km from nearest GPS station.

(cf. Appendix C). Although these tests are not representative of the whole range of possibilities, they provide a rough estimation of variability in the interseismic correction within the bounds of strong locking.

[17] The residual GPS velocities are used to derive smoothed velocity and strain rate fields (Figures 4 and 5) that provide GPS strain and seismic moment rates for comparison with seismicity. These velocity and strain rate fields (and their standard errors) are calculated using a 2-D adaptive Gaussian function applied on a regular 0.5×0.5 degree grid. The smoothing parameters are chosen to take into account the GPS station density and spatial distribution, resulting in a smoothing wavelength that varies from ~ 50 km to ~ 300 km. Details of the method and parameters are given in Appendix B.

[18] Various methods can be used to derive GPS strain rates, ranging from simple Delaunay triangulations to more complex parametric inversions [e.g., *Haines and Holt*, 1993; *Tape et al.*, 2009], with significant variations in their results. In order to assess the first-order variability in our strain rate analysis and the derived moment rates, we compute three additional strain rate fields for varying smoothing parameters (cf. Appendices B and C).

2.4. From GPS Strain Rates to Seismic Moment Rates and Gutenberg-Richter Statistics

[19] Conversions between a strain rate tensor $\dot{\epsilon}_{ij}$ and a moment rate tensor \dot{M}_{ij} are commonly based on *Kostrov* [1974]:

$$\dot{M}_{ij} = 2\mu Ah \dot{\epsilon}_{ij} \quad (4)$$

where μ and h are the assumed bulk shear modulus and seismic thickness of the crust, and A is the area of the source

zone. This equation has been used to map 2-D strain rates measured at the Earth's surface into scalar moment rates over a seismic zone volume [e.g., *Ward*, 1998a; *WGCEP*, 1995]. However, *Savage and Simpson* [1997] showed that this approach leads to a non-unique determination (and mostly under-estimation) of the scalar moment rate, due to the fact that a 2-D strain rate tensor does not typically correspond to a double-couple mechanism. They proposed a variation of equation (4) that provides a scalar moment rate \dot{M}_0 that best matches the crustal strain rate:

$$\dot{M}_0 = 2\mu Ah \text{Max}(|\dot{\epsilon}_1|, |\dot{\epsilon}_2|, |\dot{\epsilon}_1 + \dot{\epsilon}_2|) \quad (5)$$

where $\dot{\epsilon}_1$ and $\dot{\epsilon}_2$ are the principal components of the strain rate tensor, and *Max* is a function returning the largest of its arguments. We follow *Savage and Simpson's* [1997] approach to calculate a scalar strain rate (and its standard error) at each grid point within our seismic zones. We then calculate a weighted average scalar strain rate and the associated seismic moment rate for the whole zone, with their respective standard errors.

[20] Assuming that earthquake frequency-magnitude statistics follow a Gutenberg-Richter distribution (equation (1)) of given slope b and maximum magnitude M_X , the scalar seismic moment rate \dot{M}_0 can be used to estimate the seismicity level a [*Mazzotti et al.*, 2005]:

$$a = \log_{10} \left(\dot{M}_0 \frac{c-b}{b} \right) - (c-b)M_X - d \quad (6)$$

Using the smoothed GPS strain rate maps, we derive an average seismic moment rate (equation (5)) and seismicity

Table 3. GPS Strain Rates, Moment Rates, and Seismicity Levels^a

Zone	$\dot{\epsilon}^G$ (10^{-9} yr $^{-1}$)	$\dot{\epsilon}_{\min}^G$ (10^{-9} yr $^{-1}$)	$\dot{\epsilon}_{\max}^G$ (10^{-9} yr $^{-1}$)	\dot{M}_0^G (10^{17} Nm yr $^{-1}$)	$\dot{M}_{0\min}^G$ (10^{17} Nm yr $^{-1}$)	$\dot{M}_{0\max}^G$ (10^{17} Nm yr $^{-1}$)	a^G	a_{\min}^G	a_{\max}^G
QCI	9.09	5.05	13.13	6.08	3.32	12.3	3.65	3.13	4.17
NVI	8.60	5.86	11.34	13.6	8.12	23.9	3.00	2.44	3.55
FORN	2.63	0.32	4.93	1.09	0.207	4.05	2.37	1.41	3.30
FORS	2.03	0.03	4.02	0.694	0.00896	2.57	2.62	1.07	3.86
ALB	1.21	0.01	2.91	4.43	0.0441	12.8	4.92	3.66	6.43
BCN	2.43	0.33	4.53	2.48	0.408	5.79	6.08	5.28	6.44
BCS	3.17	1.36	4.98	1.82	0.976	3.65	4.19	3.52	4.85
MVI	8.75	6.65	10.84	4.54	2.97	5.98	0.85	0.33	1.38
WASH	4.25	2.16	6.34	1.86	1.16	3.44	3.77	3.18	4.33
SVI	8.83	6.99	10.68	4.09	2.73	5.21	3.34	2.70	3.98
PUG	9.60	7.73	11.48	2.82	1.90	3.52	2.87	2.52	3.23
OLY	15.72	13.32	18.12	4.07	2.99	5.44	3.40	2.45	4.37

^aZone: source zone abbreviation (Figure 1). $\dot{\epsilon}^G$: median GPS scalar strain rate (cf. section 2.4 and equation (5)). \dot{M}_0^G : median GPS-based scalar seismic moment rate. a^G : median GPS-based seismicity level (a value of Gutenberg-Richter statistics) assuming fixed b and M_x values (cf. Table 2). For each $\dot{\epsilon}^G$, \dot{M}_0^G , and a^G , the “min” and “max” values are the lower and upper bounds of the 67% confidence interval, respectively.

level (equation (6)) for each seismic zone (Table 3), with prescribed local shear modulus, seismic thickness, moment-magnitude relation, and maximum magnitude, and with b values based on the earthquake catalog analysis (Table 2). In order to account for uncertainties in these input parameters and in the GPS strain rates, we use the same logic-tree method as for the earthquake catalog analysis (section 2.2). The choice of parameter ranges and probabilities is explained in Appendix A and presented in Table 2, and the resulting seismic moment rates and GR parameters are given in Table 3.

3. Results

3.1. GPS Versus Earthquake Catalog Comparison

[21] Table 4 and Figure 6 present an overview of the comparison between GPS-based and earthquake catalog-based moment rates in terms of the ratio of GPS to catalog moment rates. In order to estimate the median and 67% confidence interval (67CI) of this ratio, we use a Monte-Carlo simulation based on 10^4 random samples of the moment rate distributions. The confidence intervals of the moment rate ratios are strongly asymmetric, with large upper bounds, due to the asymmetry of the moment rate lognormal

distributions. Comparisons of the catalog and GPS-based earthquake statistics are shown for each zone in Figure 7.

[22] As discussed in section 2, catalog b values, interseismic corrections, and strain rate mapping are subject to systematic uncertainties that are not taken into account in our logic-tree analysis. These could be incorporated into more complex logic tree or uncertainty analyses, e.g., as suggested by *Wallace et al.* [2009] and *Stirling et al.* [2009] for a case study of northern Japan. In order to assess the effects of these systematic uncertainties, we have run a series of alternative models with different b value, interseismic locking, and strain rate smoothing that are described in Appendix C. The tests are meant to provide a first-order indication of how our results may vary due to these factors. The following discussion is primarily based on the reference model, with references to the alternatives where they are significant.

[23] We find good agreement between the GPS and catalog moment rates in two zones, Puget Lowland (*PUG*) and Mid-Vancouver Island (*MVI*), with median GPS/catalog ratios of about 1 (67CI about 0.5–5). The *PUG* result is robust (Figure 7k) and confirms a previous study that identified a good fit between earthquake statistics and north-south GPS shortening rate in the Puget Lowland – southern

Table 4. GPS Versus Earthquake Catalog Moment Rates^a

Zone	\dot{M}_0^G/\dot{M}_0^S			$\dot{M}_0^G - \dot{M}_0^S$			$T^G - T^S$ (MW = 7)			T^S (MW = 7)		
	Med	Min	Max	Med (10^{17} Nm yr $^{-1}$)	Min (10^{17} Nm yr $^{-1}$)	Max (10^{17} Nm yr $^{-1}$)	Med (yr)	Min (yr)	Max (yr)	Med (yr)	Min (yr)	Max (yr)
QCI	6.0	1.4	25.6	5.06	1.08	23.71	70	15	329	348	86	1414
NVI	7.9	1.7	37.3	11.88	2.3	61.06	30	6	154	206	44	969
FORN	4.7	0.3	70.0	0.86	$>10^{-3}$	14.85	412	24	7092	1556	138	1.7×10^4
FORS	2.9	0.1	71.0	0.46	0.01	13.26	770	27	2.2×10^4	1523	250	9337
ALB	157.1	4.2	5902.4	4.40	0.10	201.40	81	2	3687	1.3×10^4	991	1.6×10^5
BCN	3×10^4	2.2	5×10^8	2.48	$>10^{-3}$	6×10^5	143	0	3.5×10^6	4.9×10^6	219	$>10^8$
BCS	19.2	2.6	135.4	1.72	0.22	13.65	206	26	1628	3727	525	2.6×10^4
MVI	1.2	0.3	5.1	0.59	0.12	2.81	601	126	2869	90	20	412
WASH	9.6	1.9	47.9	1.67	0.30	9.17	213	39	1174	1820	360	9145
SVI	8.3	1.4	47.2	3.59	0.57	22.53	99	16	619	715	118	4359
PUG	1.3	0.5	3.4	0.67	0.24	1.86	530	191	1472	165	62	437
OLY	17.8	1.4	217.0	3.84	0.28	53.08	92	7	1277	1543	114	2.1×10^4

^a \dot{M}_0^G/\dot{M}_0^S : Ratio of GPS-based to earthquake statistical seismic moment rate. \dot{M}_0^G/\dot{M}_0^S : Difference between GPS-based and earthquake statistical seismic moment rate. $T^G - T^S$ (MW = 7): Difference between GPS-based and earthquake statistical moment rate expressed as equivalent return period of $M_w = 7.0$ earthquakes. T^S (MW = 7): Catalog statistical moment rate expressed as equivalent return period of $M_w = 7.0$ earthquakes. Each parameter is presented as a median (med) and lower and upper bounds of the 67% confidence interval (min, max).

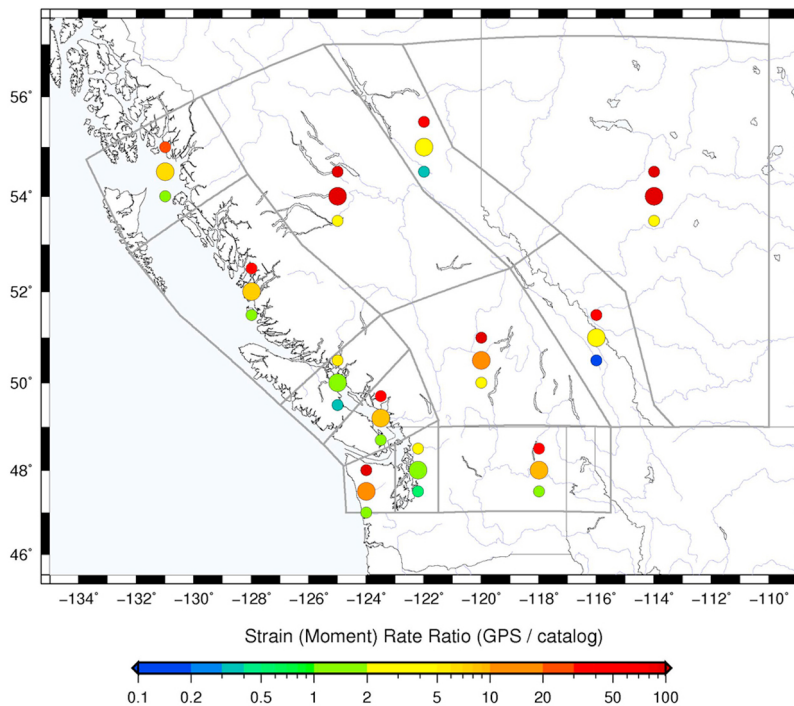


Figure 6. Ratio of GPS to catalog moment rate. Ratio of GPS-based to catalog-based seismic moment rate shown as median value (large central circle) and upper and lower bounds of 67% confidence interval (smaller upper and lower circles). Nonlinear color scale highlights variability of ratios, with green values centered on 0.5–2.0 range.

Strait of Georgia area [Hyndman *et al.*, 2003]. In contrast, results for *MVI* are less reliable because of the small number of earthquakes (Table 1) and the strong sensitivity to the *b* value and strain rate smoothing uncertainties (Appendix C). The sensitivity tests for *MVI* indicate that the medians of GPS minus catalog moment rate differences can vary by a factor of 4–10 (Figure C2).

[24] The next agreement level is found in the Foreland Belt - South zone (*FORS*), with a median GPS/catalog ratio of ~ 3 , but large upper and lower bounds (67CI 0.1–71.0). Compared to *PUG*, the larger uncertainty is a due to larger standard errors in the catalog *a* and *b* values as well as the GPS strain rate. As shown in Appendix C, the median strain rate estimate is also fairly sensitive to the smoothing parameters.

[25] In every other zone, the median GPS/catalog ratio is larger than 3. Due to poor catalog statistics and GPS data coverage, the GPS/catalog comparisons in Foreland Belt - North (*FORN*) and Central BC - North (*BCN*) are unreliable and will not be discussed further. In the remaining seven zones, the quality of the GPS/catalog comparison can be viewed as adequate (*ALB*, *FORS*, *BCS*, *WASH*, *OLY*) or good (*QCI*, *NVI*, *SVI*) on the basis of earthquake statistics, GPS data coverage, and sensitivity to the model assumptions. In these zones, the median GPS/catalog ratios range between about 6 and 20, with a lower bound larger than 1.4 (67CI about 1.4–200), except for *ALB* associated with a ratio of 157 (67CI about 4–6000).

[26] The GPS/catalog comparison can also be expressed in terms of moment rate difference (GPS minus catalog) or, for a more intuitive representation, as the return period of $M_W = 7.0$ earthquakes equivalent to the moment rate difference

(Table 4). The latter provides a measure of the number of “missing” large earthquakes necessary to match GPS moment rates to the catalog. In the two zones with good GPS/catalog agreement (*PUG* and *MVI*), the return periods of missing $M_W = 7.0$ earthquakes are long (500–600 yr) compared to the return period predicted by the catalog (100–150 yr). In the *FORS* zone, the return period of missing $M_W = 7.0$ is also long (~ 770 yr), but much shorter than the catalog one (~ 1500 yr). Elsewhere, the missing $M_W = 7.0$ return periods are short (30–200 yr) and, on average, 5–20 times shorter than the catalog ones, illustrating the lack of seismic moment in the catalog relative to the GPS.

3.2. PSHA Comparisons

[27] In order to estimate the impact of GPS strain rates on seismic hazard models, we derive and compare shaking probability maps using GPS-based and catalog-based earthquake statistical parameters (*a* and *b* GR values), as well as our assumed source zones and maximum magnitudes. The maps are calculated in a similar manner to those in the 2005 Canadian National Seismic Hazard Model [Adams and Halchuk, 2003], with the exception that we do not include source zones for the Cascadia subduction fault, Queen Charlotte fault zone, or intraslab earthquakes (i.e., we only consider crustal earthquakes). We calculate the median 5% damped peak ground acceleration (PGA) and spectral acceleration (*S_a*) at various probabilities of exceedance for both GPS-based and catalog-based statistics.

[28] As an example, Figures 8a and 8b show the median PGA at 2% in 50 years ($\sim 1/2500$ yr) exceedance, and Figure 8c shows the ratio of the GPS-based to the catalog-

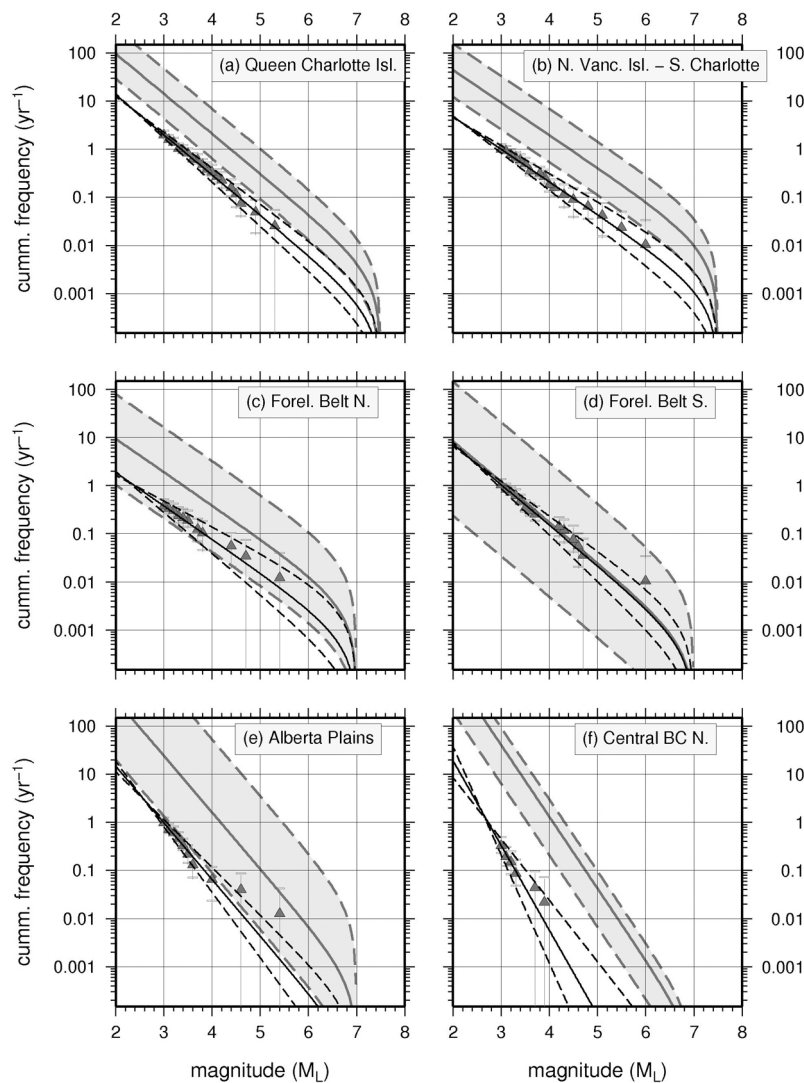


Figure 7. Earthquake catalog versus GPS frequency-magnitude statistics. Solid triangles show cumulative frequency-magnitude (Gutenberg-Richter - GR) distributions of earthquakes from GSC catalog, with associated 67% confidence intervals. Black solid and dashed lines show best fit and 67% confidence truncated GR function for earthquake catalog. Gray solid and dashed lines show predicted median and 67% confidence truncated GR function derived from GPS strain rates.

based median PGA. As expected from the moment rate comparison, the only three zones where the catalog and GPS ground-shaking probabilities agree well are *PUG*, *MVI*, and *FORS* (median ratio of 1.1–1.2). In these zones, the GPS and catalog data predict median PGA between ~ 0.3 and ~ 0.1 g. In all other zones, the median PGA ratio is about 2–3, except in *ALB* where it reaches ~ 5 . In this zone, the large ratio is due to the very low (near-zero) seismicity level, which in the catalog-based results is mapped into a “ground-floor” shaking of ~ 0.03 g median PGA (Figure 8a). In contrast, the GPS strain rates, although low, result in non-negligible ground shaking of 0.1 g. Similar results are observed for other exceedance probabilities and spectral acceleration periods.

[29] The PSHA analysis results in an overall damping of the discrepancy between GPS and catalog seismic rates. In most zones, the GPS-based moment rate (and frequency of

large earthquakes) is 6–20 times larger than the catalog-based one, whereas the resulting ground shaking is only 2–3 times larger (cf. Figure 6 versus Figure 8c). Although damped, these increases in ground shaking are significant and would represent a drastic change in hazard assessment in most of western Canada and northern Washington.

4. Discussion

[30] In all but three cases examined here, the median GPS-based moment rates are significantly larger than the median earthquake catalog-based ones (Figure 6), with GPS/catalog moment rate ratios ranging between ~ 6 and ~ 150 . Although commonly not significant with the estimated 67% confidence limits, this nearly systematic over-estimation of earthquake catalog statistics by GPS strain rates suggests a fundamental issue in the relationship between seismic strain and bulk

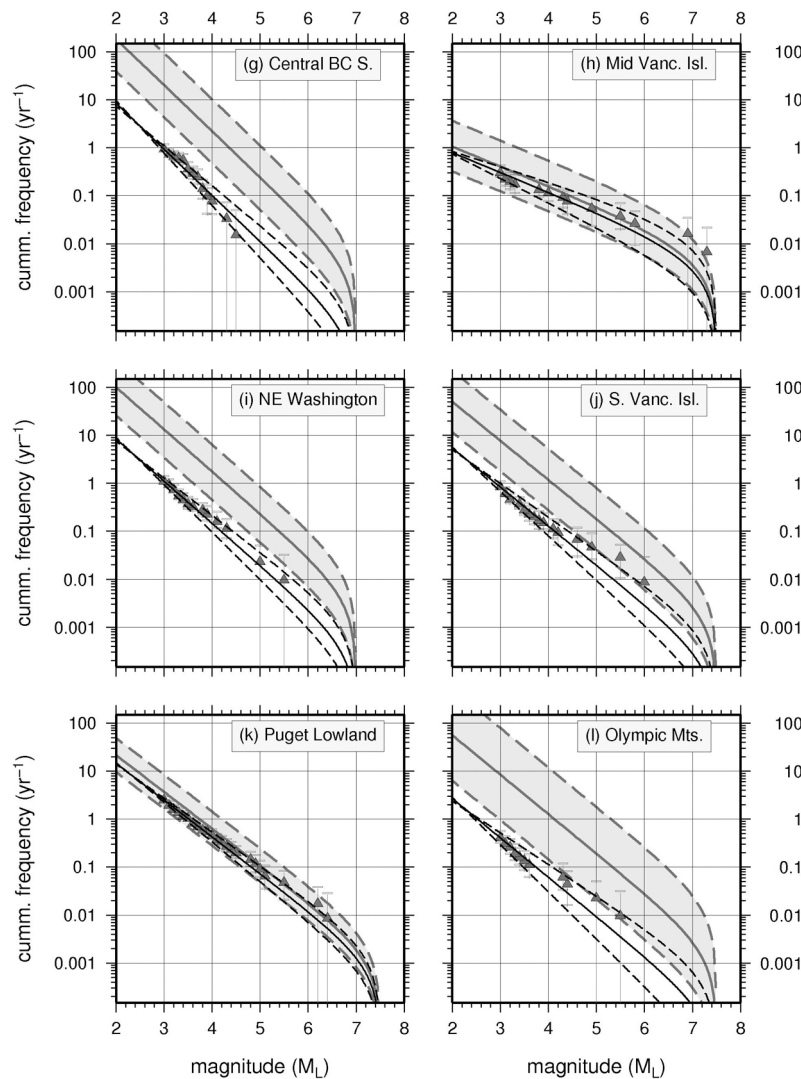


Figure 7. (continued)

crustal strain. After a brief review of other studies that have attempted a comparison of earthquake catalog and GPS strain rates, we discuss the possible causes of this GPS/catalog discrepancy and potential issues for integrating GPS strain rates into PSHA.

4.1. GPS/Seismicity Comparisons in Other Studies

[31] Several early studies have compared moment or strain rates estimated from geological data with those from earthquake catalogs. For example, *Anderson* [1979] found an overall agreement between observed catalog statistics and those derived from fault slip rates in southern California. Similarly, *Hyndman and Weichert* [1983] found that fault slip rates derived from earthquake catalogs and from plate tectonic models agreed well for offshore western Canada. However, both studies noted cases of significant disagreement between catalog statistics and geological estimates, which they attributed to aseismic deformation, elastic strain, or under-sampling of the earthquake catalog.

[32] The recent advent of high-precision geodetic data has led to numerous attempts to integrate geodetic strain data in seismicity and PSHA studies. *WGCEP* [1995] provided one of the first detailed combinations of geodetic and seismicity data in a seismic hazard analysis of southern California. They found that geodetic moment rates were in good agreement with rates derived from paleoseismicity, but systematically larger than those derived from catalogs by a factor of about two. As in most other studies, they explained this discrepancy by possible aseismic deformation, underestimation of local maximum magnitudes, or under-sampling of the earthquake catalog. In a revised analysis, *Field et al.* [1999] found that geodetic and catalog moment rates could be matched by adjusting catalog b values, magnitude-moment relations, or magnitude estimates. More recent studies provide estimates of GPS to earthquake catalog moment rate ratios that range from factors of ten and more [e.g., *Jenny et al.*, 2004; *Barani et al.*, 2010] to about one [e.g., *Mazzotti et al.*, 2005; *Grunewald and Stein*, 2006].

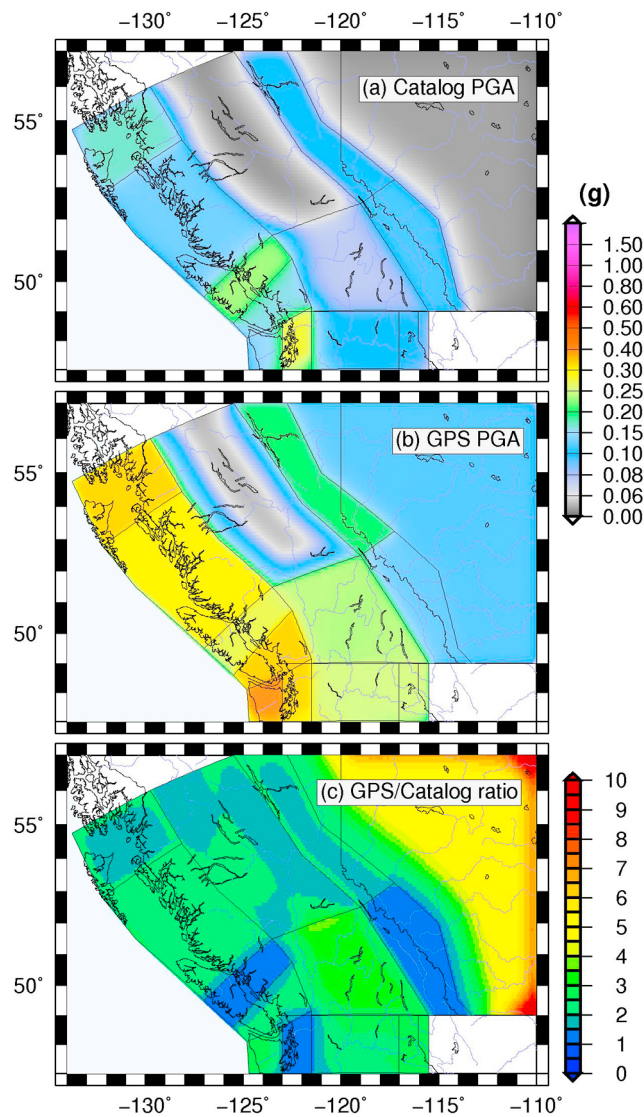


Figure 8. Ground shaking probability derived from earthquake catalog versus GPS strain rates. Peak ground acceleration (PGA) at 2% in 50 years exceedance probability from (a) the earthquake catalog and (b) GPS strain rates. (c) Ratio of GPS to catalog PGA. Note these maps are for the purpose of comparison, not for exact seismic hazard assessment.

[33] In the previous examples, the estimation of a total catalog seismic moment (or strain) rate is based on the integration of GR statistics (similar to equation (5)). In contrast, numerous studies have relied on moment summation to derive an estimate of instrumental earthquake moment rates [e.g., Ward, 1998a, 1998b; Masson *et al.*, 2005] or paleoseismic moment rates [e.g., Shen-Tu *et al.*, 1995; Hammond and Thatcher, 2004]. In nearly all cases, the comparison of these estimates with geodetic data showed that geodetic rates are systematically larger than seismicity or paleoseismicity rates by factors of 2–20 and larger. Masson *et al.* [2005] argued that the high GPS/seismic strain rate ratio in southern Iran (~ 20) is relatively steady over time periods of 100–1000 years and is not biased by catalog completeness. In contrast, Ward [1998a] suggested that the

primary cause of the GPS/seismic discrepancy in the U.S.A. may be that “seismic catalogues fail to reflect long-term earthquake rates.” The latter is supported by our comparison of observed versus statistical moment rates, which suggests that our ~ 100 -year earthquake catalog only captures 10–80% of the long-term seismicity as estimated by GR statistics.

4.2. Reconciling GPS and Catalog Moment Rates

[34] In order to reconcile the median GPS and catalog moment rates in most of the zones, the GPS rates would have to be divided by about 6–20, or the catalog rates multiplied by the same amount. Ten parameters contribute to the calculation of GPS and catalog moment rates (equations (2) and (5)). Neglecting the nonlinearity of the equations and the cross-correlations in the parameter dependencies, we can estimate the approximate change required in any one parameter in order to account for a factor of 6–20 difference in GPS and catalog moment rates. Of those ten possible changes, seven are unrealistic:

[35] 1. A factor 6–20 reduction of the GPS moment rate (equation (5)) requires a division by 6–20 of the crustal shear modulus, seismic zone area, or seismic thickness, well beyond the range of reasonable values. Crustal shear modulus variations are typically limited to 10–30% [Turcotte and Schubert, 2002]. Source zone areas are defined by their vertex coordinates. Seismic thicknesses are constrained by earthquake depth range (roughly 15–30 km) and do not vary by more than $\sim 50\%$.

[36] 2. A factor 6–20 increase of the catalog moment rate (equation (2)) requires: a magnitude-moment parameter increase (d by about 0.8–1.3 or c by about 0.1–0.2) much larger than those permitted by earthquake data [Ristau *et al.*, 2005]; a multiplication of the asymmetry factor ϕ by 6–20, well beyond the range of magnitude uncertainties [e.g., Hyndman and Weichert, 1983]; or a maximum magnitude increase of about 1.1–1.8, leading to unrealistic $M_X = 8.1$ –9.3.

[37] The last point regarding maximum magnitudes is justified by the maximum dimension of known active faults and other geological structures, which remain below 100–150 km in our study area, thus defining M_X values of about 7.0–7.5 [Adams and Halchuk, 2003; Petersen *et al.*, 2008]. Typical scaling relationships for $M_W \geq 8.0$ require either a very long and thin rupture (e.g., 400×15 km) or a shorter rupture through the entire crust (e.g., 200×30 km). Contrary to other plate-boundary zones such as California or New Zealand, western Canada – northwestern U.S. has no indication of onshore surface ruptures on long, mature active fault systems, which leads us to conclude that $M_X \geq 8.0$ is unrealistic in the region as a whole (although not impossible in a few limited locations). However, we recognize that the definition of M_X remains a debated topic and that higher M_X values could be considered in more in-depth analyses.

[38] Some combinations of more reasonable variations in these parameters could lead to agreement between GPS and catalog moment rates. However, reasonable uncertainties are already taken into account in both estimates through formal uncertainty propagation or logic-tree analysis (section 2). These do not result in the systematic discrepancies observed between GPS and catalog rates.

[39] The remaining three parameters (GPS strain rate and catalog a and b values) are discussed independently as they

relate to more conceptual issues with the GPS/catalog comparison.

4.3. GPS Strain Rate and Aseismic Deformation

[40] Visco-elastic response of the lithosphere to postglacial rebound (PGR) since the last Ice Age is a common source of aseismic strain. Numerical models and direct GPS measurements indicate that PGR elastic strain rates can reach $1\text{--}10 \times 10^{-9} \text{ yr}^{-1}$ in central and eastern Canada, mainly due to the slow response of the cold lithosphere and asthenosphere [e.g., *James and Bent, 1994; Calais et al., 2006*]. The GPS strain rate measured for the zone Alberta Plains (*ALB*) may partly or fully represent aseismic PGR deformation, thus accounting for the large difference between GPS and catalog moment rates in this zone. In contrast, present-day PGR is insignificant in the Canadian Cordillera, due to the fast response time of the low-viscosity asthenosphere [e.g., *James et al., 2009*]. Thus, in all zones except *ALB*, PGR strain rates are likely negligible and do not contribute significant aseismic strain to the GPS measurements.

[41] Another source of aseismic deformation is the visco-elastic loading and relaxation of the crust and mantle during earthquake cycles on large faults, which affect GPS stations located within a few fault-lengths of these faults. For the most recent large earthquakes capable of generating significant postseismic deformation ($M_W \sim 9.0$, 1700 Cascadia, $M_W = 8.1$, 1949 Queen Charlotte, and $M_W = 7.3$, 1946 Vancouver Island), present-day GPS and numerical models indicate that postseismic strain rates are currently negligible [*Hippchen and Mazzotti, 2010; Mazzotti et al., 2003a, 2003b; Wang et al., 2003*]. As described in section 2.2, we correct the GPS velocity data for predicted interseismic loading from the Queen Charlotte and Cascadia plate-boundary faults. These corrections tend to reduce the GPS strain rates and are unlikely to be the source of a factor of 6–20 over-estimation. Our test results for two alternative interseismic models show that the impacts on GPS moment rates and the GPS/catalog ratios are limited to $\pm 10\%$ on average and $\pm 50\%$ maximum, well below the factor of 6–20 required to match GPS and catalog seismic moment rates (Appendix C).

[42] Alternatively, more complex models of interseismic locking coupled with rotations of crustal blocks have been proposed to explain the GPS velocity variance in terms of variable interseismic deformation and rigid block rotations, with or without intrablock strain. Arguably, the GPS velocities of the Vancouver Island and Queen Charlotte margins can be modeled as rigid block rotation with little internal strain [*McCaffrey et al., 2007; Elliott et al., 2010*]. Detailed analyses of these model predictions versus earthquake moment rates would be required to quantify the potential improvement compared to our distributed strain approach. However, these models produce strain concentrations (high fault slip rates) along the block edges, pushing the issue of GPS versus seismic moment rates from inside the blocks to narrow bands along the block margins, which do not show high earthquake concentrations.

[43] Finally, long-term bulk aseismic deformation or creep may result in an over-estimation of seismic moment rates from GPS measurements. Only a few well-documented cases exist of long-term aseismic creep along large mature

faults (e.g., San Andreas Fault [*Moore and Rymer, 2007*]). Although this type of long-term creep has been proposed as an explanation for the difference between GPS and seismic rates in some areas [e.g., *WGCEP, 1995; Masson et al., 2005; Barani et al., 2010*], most studies remain susceptible to limitations due to catalog completeness or geodetic strain rate resolution, thus providing limited evidence that this process may be a common mode of deformation.

4.4. Earthquake Catalog Versus Long-Term Seismicity

[44] The integration of a 50–100 yearlong earthquake catalog to derive statistical seismic moment rates (or ground-shaking probabilities) relies on the assumption that the catalog represents a temporally stable and adequate sample of long-term seismicity. This is commonly addressed by assuming that earthquake distribution is ergodic over large, rapidly deforming regions [e.g., *Smith, 1976; Ward, 1998a*]. Using the Basin and Range example, *Panchar et al. [2006]* propose an empirical measure of the minimum catalog duration T (yr) required for a valid ergodicity assumption in a region of area A (km^2) and average strain rate $\dot{\epsilon}$ (yr^{-1}):

$$T \geq \frac{1.5}{A\dot{\epsilon}} \quad (7)$$

Using this expression and our GPS strain rates, the required catalog durations for our twelve seismic zones range between ~ 900 and ~ 6000 years, in all cases much longer than the actual catalog time span. This would suggest that an ergodic substitution requires catalogs about 10–100 times longer than currently exist, even in the largest zones. However, we find the best GPS/catalog agreement in Puget Lowland, one of the smallest zones of our study area. Using this zone as a proxy for the adequate catalog duration, equation (7) becomes:

$$T \geq \frac{0.025}{A\dot{\epsilon}} \quad (8)$$

and the required catalog durations for our eleven other zones range between ~ 20 and ~ 100 years. This simple analysis illustrates the difficulty of a robust quantification of the ergodicity argument.

[45] More qualitative arguments can be made to suggest that earthquake catalog representativity is likely not the overall cause of the 6–20 GPS/catalog ratios. Accounting for this difference requires either a systematic increase in the catalog seismicity level (a value) of about 0.8–1.3 or a systematic decrease of the b value by about 0.1–0.2. The latter is within the standard error estimated for most zones (Table 3), but it corresponds to a large increase in the predicted recurrence rate of $M \geq 6.0$ earthquakes by a factor of about 5–15. The fixed b value test (Appendix C) also shows that using a uniform regional b value has a very small effect on our results (less than 30%, Figure C2), except for the mid Vancouver Island zone where the fixed GR grossly misfits the earthquake catalog. Similarly, the required a value increase represents about 6–20 times more earthquakes over the whole magnitude range, and it is much larger than the estimated standard errors (Table 1). In both cases, it is unlikely that the catalog snapshot happens to systematically sample a period of ten-fold lower seismicity level in nearly all of our study area.

[46] The argument of the under-sampling of the earthquake catalog can also be considered from the perspective of

missing large characteristic earthquakes, i.e., events that do not follow the regional GR distribution. Table 4 lists the return periods of missing characteristic $M_W = 7.0$ earthquakes required to account for the GPS/catalog discrepancy. These return periods range between ~ 30 and ~ 770 years. Taken individually in each zone, the ~ 100 yearlong catalog could conceivably lack $M_W = 7.0$ earthquakes with a return period of the same order as, or longer than the catalog length. However, when taken over the whole study area, the systematic GPS/catalog mismatch requires the unrealistic scenario wherein about 11 $M_W = 7.0$ earthquakes would be missing from the whole catalog (i.e., one $M_W = 7.0$ every 10 years).

4.5. Issues and Requirements for GPS-PSHA Integration

[47] The zone *ALB* is the only one for which we can propose a single reasonable explanation for the GPS/catalog mismatch. There, as in several other continental intraplate regions (e.g., northern Europe), viscoelastic postglacial rebound strain rates exceed seismic strain rates by a factor of 10 or more [e.g., *James and Bent*, 1994] and represent the primary deformation measured by GPS. Thus, for those intraplate regions, GPS strain rate data provide a maximum, unrealistically high estimate of the potential seismic moment rate, and are of limited value for PSHA analysis. In continental intraplate regions not affected by PGR (e.g., Australia), or where the seismic strain signal could be untangled from the PGR one on the basis of spatial wavelength, GPS data may provide useful constraints in zones of concentrated seismicity [*Mazzotti*, 2007].

[48] In contrast, the zone *PUG* provides an example where GPS and catalog rates corroborate each other, thus providing a higher level of confidence in PSHA results derived from the combination of both data sets. This zone is characterized by the highest seismic activity of our entire study area (Figure 2), and by a series of large crustal faults that account for the seismic and geodetic strain rates [*Sherrod et al.*, 2008]. Similarly, other regions with reasonable GPS/earthquake catalog agreements tend to be associated with high seismicity levels and large crustal faults (e.g., California [*Anderson*, 1979; *Field et al.*, 1999]). In contrast, most of our study area is characterized by lower seismicity levels and the absence of large mature active faults. Under these conditions, the high GPS/catalog moment rate ratios may be reconciled through a combination of biased earthquake catalog statistics, over-estimated GPS strain rates (due to mis-modeling of the plate-boundary interseismic strain or rigid-block tectonics), and, arguably, long-term aseismic deformation of the crust on a regional scale.

[49] Although it cannot be demonstrated with a significant level of confidence on the basis of our results, long-term aseismic deformation may be an important mechanism accommodating a large portion of the crustal deformation in low-seismicity, active tectonic regions. Our analysis of catalog seismicity versus GPS suggests that aseismic deformation may account for up to 80–90% of the total crustal deformation in a significant portion of the western Canadian Cordillera (Figure 5). In order to use GPS strain rates in PSHA analysis, the seismic versus aseismic portions of the crustal deformation budget need to be quantified. This requires a better understanding of the physical and mechanical conditions leading to mainly seismic (e.g., *PUG*)

versus mainly aseismic (e.g., *QCI*) strain budgets. These requirements can only be addressed through more detailed and higher resolution comparative and modeling studies of GPS and seismic rates.

5. Conclusion

[50] We tested an alternative approach to assess seismic hazard in western Canada and northwestern U.S.A. using GPS strain rate data to derive seismic moment rates and ground shaking probabilities in seismic source zones. In two zones (Puget Lowland and Mid-Vancouver Island), the median GPS-based moment rate and PSHA estimates are in good agreement with those derived from the earthquake catalogs. In seven other zones, the median GPS-based moment rates are 6–150 times larger than those from the earthquake catalogs, and the PSHA estimates are 2–5 times larger, although in most cases the GPS and catalog results agree within the estimated 67% confidence intervals. In individual source zones, this discrepancy may be explained by the ~ 100 yearlong earthquake catalog significantly under-predicting long-term earthquake statistics, and thus hazard. However, this explanation is unreasonable on the scale of the entire study area, as it would require the equivalent of about one additional $M_W = 7.0$ earthquake every 10 years (i.e., 11 missing events in the entire catalog). Long-term aseismic crustal deformation could account for the observed GPS/catalog discrepancies, providing it represents up to 80–90% of the total deformation budget in some of the seismic zones.

[51] Aseismic deformation is a reasonable explanation for formerly glaciated continental intraplate regions (e.g., Alberta Plains), where most of the GPS strain rate signal likely comes from aseismic postglacial rebound. In these regions, GPS strain rates provide a maximum estimate of potential seismic hazard, although likely too high to be useful. On a longer geological time-scale, aseismic deformation may also be prevalent in active plate-boundary regions characterized by low-magnitude background seismicity or a lack of large, mature active faults, such as the Queen Charlotte margin or the Zagros belt in southern Iran [*Masson et al.*, 2005]. In contrast, regions with high seismicity level and numerous large faults may be associated with deformation that is mainly seismic (e.g., Puget Lowland, southern California).

[52] GPS strain rates can provide an important and useful complement to earthquake catalog statistics for seismic hazard analysis, for example through formal integration of several GPS strain rate and tectonic models using a logic-tree approach [e.g., *Stirling et al.*, 2009]. However, significant research is required to better understand the limitations and applicability of GPS strain rates, especially regarding the possibility of large aseismic deformation on long-term regional scales. Similar studies in other regions are required to define and validate this approach, with the goal of developing guidelines that can be used in projects such as the Global Earthquake Model (<http://www.globalquakemodel.org/>).

Appendix A: Seismic Moment Rate Parameters

[53] In order to estimate the median and uncertainty range of seismic moment rates derived from GPS strain rates

(equation (5)) and earthquake catalog data (equation (2)), we use a logic tree approach using a lower, a median, and an upper value (with their associated probabilities) for each set of parameters [Mazzotti and Adams, 2005; Mazzotti et al., 2005]. The choices of parameters and probabilities are listed in Table 2. In each case, we choose a three-point discrete probability distribution for the lower, median, and upper parameters reflecting either a Gaussian distribution (0.75, 0.45, 0.275) or a slightly broader distribution (0.3, 0.4, 0.3) for more uncertain cases.

[54] 1. Crustal shear modulus (μ): We use a median value of 3.0×10^{10} N/m², typical of average crustal rocks [Turcotte and Schubert, 2002], and allow for a 23% variation for the lower and upper ranges, in association with a Gaussian probability distribution.

[55] 2. Seismic thickness (h): We use three seismic thickness ranges depending on the regional thermal regime of the crust [cf. Hyndman et al., 2005; Mazzotti et al., 2008]. Regions in the subduction zone forearc (*OLY*, *PUG*, *SVI*, *MVI*) and in the Craton (*ALB*) are associated with a cold geotherm and a median seismic depth of 25 km (20/30 km – lower/upper bounds). Regions in the Cordillera (*BCN*, *BCS*, *WASH*) are associated with a hot geotherm and a median seismic depth of 12 km (10/15 km). In other regions, the seismic depth is less well defined, and is associated with a median of 20 km and a wide range (10/30 km). In all cases, we use the broad probability distribution.

[56] 3. Source zone area (A): The source zone area is the area of the spherical cap defined by the coordinates of the zone vertices.

[57] 4. Strain rates ($\dot{\epsilon}^G$): The estimation of the median scalar strain rate and its standard error in each zone is described in section 2.4. Lower, median, and upper values are given in Table 3. The associated probability distribution is Gaussian.

[58] 5. Magnitude - moment asymmetry correction (ϕ): We use the estimation of 1.27 (± 0.2 magnitude unit variance) of Hyndman and Weichert [1983] for western Canada earthquakes as our median value, allowing for a range of ± 0.1 and ± 0.3 magnitude units that define lower and upper bounds of 1.06 and 1.71, with a Gaussian probability distribution.

[59] 6. Magnitude - moment conversion (c and d): We use the magnitude - moment relation calibrated by Ristau et al. [2005] for western Canada earthquakes ($c = 1.5$, $d = 9.05$), allowing for a 0.10 variation in d , equivalent to ~ 0.07 magnitude units. The associated probability distribution is Gaussian.

[60] 7. Maximum magnitude (M_X): We use two ranges of maximum magnitude depending on the seismic activity, seismic thickness, and magnitude distribution in the source zones. These magnitudes are updated from the 2005 Canadian and 2008 U.S. National Seismic Hazard Maps [Adams and Halchuk, 2003; Petersen et al., 2008]. For source

zones along the main plate boundary zones (Queen Charlotte and Cascadia margins), the median maximum magnitude is 7.5, with a range of ± 0.3 . For source zones farther in the interior, the median maximum magnitude is smaller (7.0) and the range slightly broader (± 0.5). In all cases, we use the broad probability distribution.

Appendix B: GPS Strain Rate Mapping

[61] The interpolated and smoothed velocity and strain rate fields are calculated using a 2-D adaptive Gaussian function applied on a regular 0.5×0.5 degree grid. At each grid point g , the velocity vector V_g is defined as the weighted average of all N GPS velocity vectors V_n weighted according to their standard errors σ_n , their distance to the grid point Δ_{ng} , and the azimuthal density of GPS data $1/K_{ng}(\omega)$:

$$V_{gi} = \left(\sum_{n=1}^N \frac{G_{ng} \Omega_{ng}}{\sigma_{ni}} V_{ni} \right) / W_i$$

with

$$G_{ng} = e^{-\log(2) \frac{\Delta_{ng}^2}{r_g^2}}$$

$$\Omega_{ng} = 1/K_{ng}(\omega)$$

$$W_i = \sum_{n=1}^N \frac{G_{ng} \Omega_{ng}}{\sigma_{ni}} \quad (\text{B1})$$

where i is the velocity component (north, east, or up), r_g is the smoothing distance (Gaussian half-width) at the grid point g , and $K_{ng}(\omega)$ is the number of GPS points inside the angular quadrant with an apex at the grid point g , of width ω , and centered on the data point n .

[62] For each grid point, the smoothing distance r_g (km) is defined as the minimum of a fixed distance D_S or the distance to the N_S^{th} nearest GPS site. Thus, the smoothing distance is adapted to the GPS station density. We choose a preferred smoothing distance ($D_S = 50$ km, $N_S = 5$) that optimizes spatial resolution without producing short wavelength artifacts, providing smoothed velocity and strain rate fields with a wavelength varying from 50–75 km in dense areas (south Vancouver Island) to 250–300 km in low density areas (northern British Columbia). Additional smoothing parameters ($D_S = 30$ km, $N_S = 2$ and $D_S = 100$ km, $N_S = 8$) are tested to assess the sensitivity of the results to the smoothing procedure.

[63] The azimuthal density factor $1/K_{ng}(\omega)$ corrects for large heterogeneities in the GPS site distributions around each grid point by increasing (decreasing) the weight of velocity vectors that are within a low (high) density quadrant. We choose a preferred quadrant width $\omega = 45^\circ$, with an additional width ($\omega = 90^\circ$) also tested.

[64] The horizontal strain rate tensor $\dot{\epsilon}_{ij}$ is defined as the spatial derivative of the Gaussian velocity function evaluated at the grid point g :

$$\dot{\epsilon}_{ij} = \frac{\log(2)}{r_g^2} \left[\left[\left(\sum_{n=1}^N - \Delta_{jg} \frac{G_{ng} \Omega_{ng}}{\sigma_{ni}} V_{ni} \right) / W_i - \left(\sum_{n=1}^N - \Delta_{jg} \frac{G_{ng} \Omega_{ng}}{\sigma_{ni}} \frac{V_{gi}}{W_j} \right) \right] \right. \\ \left. + \left[\left(\sum_{n=1}^N - \Delta_{ig} \frac{G_{ng} \Omega_{ng}}{\sigma_{nj}} V_{nj} \right) / W_j - \left(\sum_{n=1}^N - \Delta_{ig} \frac{G_{ng} \Omega_{ng}}{\sigma_{nj}} \frac{V_{gi}}{W_i} \right) \right] \right] \quad (\text{B2})$$

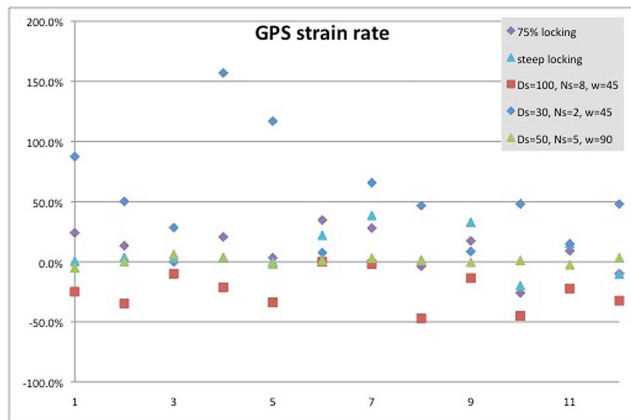


Figure C1. Strain rate variability. Variations in average scalar strain rate in each source zone expressed as a percentage relative to the reference model ($(\text{test} - \text{reference})/\text{reference}$). Source zones from 1 to 12 follow the order in Tables 1 and 2.

where $\Delta_{(i,j)g}$ is the distance in the east or north direction, and the other parameters are defined in equation (B1).

[65] For each grid point, we calculate the standard errors on the velocity vector and strain rate tensor components using a Monte Carlo simulation that takes into account the velocity standard errors as well as the density and coherence of the nearby GPS velocities. We create 5,000 samples by randomly sampling the GPS velocities within their uncertainty ranges (assuming a Gaussian distribution) and applying a random bootstrap to the original velocities. These random samples are used to calculate the standard errors on each parameter (V_{gi} and $\dot{\epsilon}_{ij}$), which are then scaled by the density of nearby GPS stations relative to the smoothing wavelength to provide the final standard errors on the gridded velocities and strain rates.

Appendix C: Sensitivity Analysis

[66] As discussed in sections 2.2 and 2.3, we test the sensitivity of our results to systematic uncertainties on the earthquake catalog Gutenberg-Richter distribution, interseismic locking models, and strain rate mapping techniques using several alternative models that fall into three categories listed below. The model results are shown in Figures C1 and C2. Figure C1 compares the median strain rates of the alternative and reference models in terms of percentage deviation from the reference ($(\text{test} - \text{reference})/\text{reference}$). Figure C2 compares the median differences (GPS minus catalog) in moment rates of the alternative and reference models in terms of percentage deviation from the reference ($(\text{test} - \text{reference})/\text{reference}$).

C1. Interseismic Locking

[67] In addition to the reference case with 100% uniform interseismic locking, we test two models with a uniform locking of 75% and a steep downdip decrease of the locking profile ($\gamma = 0.2$) [Wang *et al.*, 2003]. Both models result in smaller interseismic locking and in residual GPS strain rates larger than the reference model ones by $\sim 10\%$ on average. A few cases show strain rates smaller or larger by up to 30%

(Figure C1). Differences in moment rates (GPS minus catalog) show similar trends (Figure C2), with variations from the reference model between -40% and $+50\%$. Thus, the effect of the interseismic model variations are limited and do not impact our main results by more than 10–20% on average and 50% maximum. However, these two test cases are not exhaustive; additional models that include spatial variations in locking, and possibly in fault slip rates, should be considered for further in-depth analysis.

C2. Strain Rate Smoothing

[68] We test three alternative smoothing models ($D_S = 30$ km, $N_S = 3$, $\omega = 45^\circ$; $D_S = 100$ km, $N_S = 8$, $\omega = 45^\circ$; $D_S = 50$ km, $N_S = 5$, $\omega = 90^\circ$) that represent low smoothing, strong smoothing, and strong azimuthal density weighting, respectively (cf. Appendix A). As shown in Figures C1 and C2, the azimuthal density parameter has very little effect (variations less than $\pm 10\%$). The strong smoothing model results in strain rates smaller than the reference case by 0–50% and moment rate differences between GPS and catalog that are reduced by 0–85%. The low smoothing model yields GPS strain rates larger than the reference case by 10–180% and moment rate differences between GPS and catalog increased by 10–400%. In both cases, the mid Vancouver Island zone (#8) shows the largest change in GPS - catalog moment difference. In all other zones, the variations relative to the reference model are less than 100%.

C3. Fixed b Value

[69] This approach assumes that the number of earthquakes is too small to properly define the b value of the GR distribution in each source zone. Rather than solving for both a and b values, we solve for the a value assuming a fixed $b = 0.8$, which is the average for the whole catalog. The effect on the GPS - catalog moment differences are less than 30% in all but two zones (Figure C2). The most

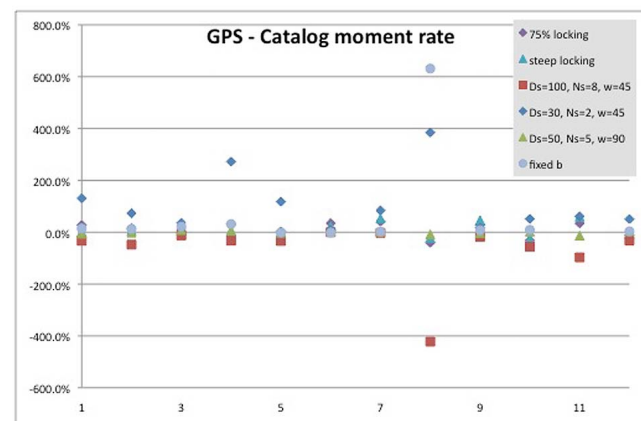


Figure C2. GPS minus catalog moment rate variability. Variations in the median differences between GPS and catalog moment rate in each source zone expressed as a percentage relative to the reference model ($(\text{test} - \text{reference})/\text{reference}$). Source zones from 1 to 12 follow the order in Tables 1 and 2.

affected zone is mid Vancouver Island (#8), where the fixed b value grossly misfits the catalog data and results in an increase in the GPS - catalog difference of $\sim 600\%$. The other large increase ($\sim 200\%$) is for the Puget Lowland zone (#11).

[70] **Acknowledgments.** Comments and suggestions by Laura Wallace and an anonymous reviewer greatly helped improve this study. We thank John Adams, Roy Hyndman and Herb Dragert, as well as colleagues at BC Hydro, W. Lettis Assoc., and URS Corp. for stimulating discussions during this project. GPS data acquisition and processing was supported by the Canadian Crustal Deformation Service (NRCan). U.S. GPS data are from the Pacific Northwest Geodetic Array and Plate Boundary Observatory projects. Figures 1–8, C1, and C2 were made using Generic Mapping Tools GMT4.5 [Wessel and Smith, 1998]. GSC contribution 20110036.

References

- Adams, J., and S. Halchuk (2003), Fourth generation seismic hazard maps of Canada: Values for over 650 Canadian localities intended for the 2005 National Building Code of Canada, *Geol. Surv. Can. Open File*, 4459, 155 pp.
- Anderson, J. G. (1979), Estimating the seismicity from geological structure for seismic-risk studies, *Bull. Seismol. Soc. Am.*, *69*, 135–158.
- Barani, S., D. Scafidì, and C. Eva (2010), Strain rates in northwestern Italy from spatially smoothed seismicity, *J. Geophys. Res.*, *115*, B07302, doi:10.1029/2009JB006637.
- Calais, E., J. Y. Han, C. DeMets, and J. M. Nocquet (2006), Deformation of the North American plate interior from a decade of continuous GPS measurements, *J. Geophys. Res.*, *111*, B06402, doi:10.1029/2005JB004253.
- Earthquake Engineering Research Institute Committee on Earthquake Risk (1989), The basis of seismic risk analysis, *Earthquake Spectra*, *5*, 675–702, doi:10.1193/1.1585549.
- Elliott, J. L., C. F. Larsen, J. T. Freymueller, and R. J. Motyka (2010), Tectonic block motion and glacial isostatic adjustment in southeast Alaska and adjacent Canada constrained by GPS measurements, *J. Geophys. Res.*, *115*, B09407, doi:10.1029/2009JB007139.
- Field, E., D. D. Jackson, and J. F. Dolan (1999), A mutually consistent seismic-hazard source model for southern California, *Bull. Seismol. Soc. Am.*, *89*, 559–578.
- Grunewald, E. D., and R. S. Stein (2006), A new 1649–1884 catalog of destructive earthquakes near Tokyo and implications for the long-term seismic process, *J. Geophys. Res.*, *111*, B12306, doi:10.1029/2005JB004059.
- Haines, A. J., and W. E. Holt (1993), A procedure for obtaining the complete horizontal motions within zones of distributed deformation from the inversion of strain rate data, *J. Geophys. Res.*, *98*, 12,057–12,082, doi:10.1029/93JB00892.
- Hammond, W. C., and W. Thatcher (2004), Contemporary tectonic deformation of the Basin and Range province, western United States: 10 years of observation with the Global Positioning System, *J. Geophys. Res.*, *109*, B08403, doi:10.1029/2003JB002746.
- Henton, J. A., M. R. Craymer, R. Ferland, H. Dragert, S. Mazzotti, and D. L. Forbes (2006), Crustal motion and deformation monitoring of the Canadian landmass, *Geomatica*, *60*, 173–191.
- Hippchen, S., and S. Mazzotti (2010), Strain partitioning, current tectonics and deformation on the southern Queen Charlotte fault, northern Vancouver Island, and the adjacent mainland, Abstract G42A-05 presented at 2010 Fall Meeting, AGU, San Francisco, Calif., 13–17 Dec.
- Hyndman, R. D., and D. H. Weichert (1983), Seismicity and rates of relative plate motion on the plate boundaries of western North America, *Geophys. J. R. Astron. Soc.*, *72*, 59–82.
- Hyndman, R. D., S. Mazzotti, D. H. Weichert, and G. C. Rogers (2003), Frequency of large crustal earthquakes in Puget Sound–Southern Georgia Strait predicted from geodetic and geological deformation rates, *J. Geophys. Res.*, *108*(B1), 2033, doi:10.1029/2001JB001710.
- Hyndman, R. D., C. A. Currie, and S. Mazzotti (2005), Subduction zone backarcs, mobile belts, and orogenic heat, *GSA Today*, *15*, 4–10, doi:10.1130/1052-5173.
- James, T. S., and A. L. Bent (1994), A comparison of eastern North America seismic strain rates to postglacial rebound strain rates, *Geophys. Res. Lett.*, *21*, 2127–2130, doi:10.1029/94GL01854.
- James, T. S., E. J. Gowan, I. Wada, and K. Wang (2009), Viscosity of the asthenosphere from glacial isostatic adjustment and subduction dynamics at the northern Cascadia subduction zone, British Columbia, Canada, *J. Geophys. Res.*, *114*, B04405, doi:10.1029/2008JB006077.
- Jenny, S., S. Goes, D. Giardini, and H. G. Kahle (2004), Earthquake recurrence parameters from seismic and geodetic strain rates in eastern Mediterranean, *Geophys. J. Int.*, *157*, 1331–1347, doi:10.1111/j.1365-246X.2004.02261.x.
- Kostrov, V. V. (1974), Seismic moment and energy of earthquakes, and seismic flow of rocks, *Izv. Acad. Sci. SSR Phys. Solid Earth*, *1*, 23–40.
- Leonard, L. J., R. D. Hyndman, S. Mazzotti, L. Nykolaishen, M. Schmidt, and S. Hippchen (2007), Current deformation in the northern Canadian Cordillera inferred from GPS measurements, *J. Geophys. Res.*, *112*, B11401, doi:10.1029/2007JB005061.
- Masson, F., J. Chéry, D. Hatzfeld, J. Martinod, P. Vernant, F. Tavakoli, and M. Ghafoory-Ashtiani (2005), Seismic versus aseismic deformation in Iran inferred from earthquakes and geodetic data, *Geophys. J. Int.*, *160*, 217–226, doi:10.1111/j.1365-246X.2004.02465.x.
- Mazzotti, S. (2007), Geodynamic models for earthquake studies in intraplate North America, in *Continental Intraplate Earthquakes: Science, Hazard, and Policy Issues*, edited by S. Stein and S. Mazzotti, *Geol. Soc. Am. Spec. Pap.*, *425*, 17–33, doi:10.1130/2007.2425(02).
- Mazzotti, S., and J. Adams (2005), Rates and uncertainties on seismic moment and deformation rates in eastern Canada, *J. Geophys. Res.*, *110*, B09301, doi:10.1029/2004JB003510.
- Mazzotti, S., R. D. Hyndman, P. Flück, A. J. Smith, and M. Schmidt (2003a), Distribution of the Pacific/North America motion in the Queen Charlotte Islands–S. Alaska plate boundary zone, *Geophys. Res. Lett.*, *30*(14), 1762, doi:10.1029/2003GL017586.
- Mazzotti, S., H. Dragert, J. A. Henton, M. Schmidt, R. D. Hyndman, T. S. James, Y. Lu, and M. Craymer (2003b), Current tectonics of northern Cascadia from a decade of GPS measurements, *J. Geophys. Res.*, *108*(B12), 2554, doi:10.1029/2003JB002653.
- Mazzotti, S., T. S. James, J. Henton, and J. Adams (2005), GPS crustal strain, postglacial rebound, and seismicity in eastern North America: The St Lawrence valley example, *J. Geophys. Res.*, *110*, B11301, doi:10.1029/2004JB003590.
- Mazzotti, S., L. J. Leonard, R. D. Hyndman, and J. F. Cassidy (2008), Tectonics, dynamics, and seismic hazard in the Canada–Alaska Cordillera, in *Active Tectonics and Seismic Potential of Alaska*, *Geophys. Monogr. Ser.*, vol. 179, edited by J. T. Freymueller et al., pp. 297–319, AGU, Washington, D. C., doi:10.1029/179GM17.
- McCaffrey, R., A. I. Qamar, R. W. King, R. Wells, G. Khazaradze, C. A. Williams, C. W. Stevens, J. J. Vollick, and P. C. Zwick (2007), Fault locking, block rotation and crustal deformation in the Pacific Northwest, *Geophys. J. Int.*, *169*, 1315–1340, doi:10.1111/j.1365-246X.2007.03371.x.
- Moore, D. E., and M. J. Rymer (2007), Talc-bearing serpentinite and the creeping section of the San Andreas fault, *Nature*, *448*, 795–797, doi:10.1038/nature06064.
- Pancha, A., J. G. Anderson, and C. Kreemer (2006), Comparison of seismic and geodetic scalar moment rates across the Basin and Range Province, *Bull. Seismol. Soc. Am.*, *96*, 11–32, doi:10.1785/0120040166.
- Petersen, M. D., et al. (2008), Documentation for the 2008 update of the United States national seismic hazard maps, *U.S. Geol. Surv. Open File Rep.*, 2008–1128, 128 pp.
- Ristau, J., G. C. Rogers, and J. F. Cassidy (2005), Moment magnitude–local magnitude calibration for earthquakes in western Canada, *Bull. Seismol. Soc. Am.*, *95*, 1994–2000, doi:10.1785/0120050028.
- Savage, J. C., and R. W. Simpson (1997), Surface strain accumulation and the seismic moment tensor, *Bull. Seismol. Soc. Am.*, *87*, 1345–1353.
- Shen-Tu, B., W. E. Holt, and A. J. Haines (1995), Intraplate deformation of the Japanese Island: A kinematic study of intraplate deformation at a convergent plate margin, *J. Geophys. Res.*, *100*, 24,275–24,293, doi:10.1029/95JB02842.
- Sherrod, B. L., S. Mazzotti, and R. Haugerud (2008), Comparison of geodetic and paleoseismic rates of deformation in the Puget Sound–Georgia Basin, Pacific Northwest, *Eos Trans. AGU*, *89*(53), Fall Meet. Suppl., Abstract T21B-1953.
- Smith, S. W. (1976), Determination of maximum earthquake magnitude, *Geophys. Res. Lett.*, *3*, 351–354, doi:10.1029/GL003i006p00351.
- Stirling, M. W., K. Berryman, L. M. Wallace, N. Litchfield, J. Beavan, and W. Smith (2009), Multidisciplinary probabilistic tectonic hazard analysis, in *Volcanism, Tectonism and Siting of Nuclear Facilities*, edited by C. Connor, L. Connor, and N. Chapman, chap. 19, pp. 257–275, Cambridge Univ. Press, Cambridge, U. K.
- Tape, C., P. Musé, M. Simons, D. Dong, and F. Webb (2009), Multiscale estimation of GPS velocity fields, *Geophys. J. Int.*, *179*, 945–971, doi:10.1111/j.1365-246X.2009.04337.x.
- Turcotte, D. L., and G. Schubert (2002), *Geodynamics*, 456 pp., Cambridge Univ. Press, Cambridge, U. K.
- U.S. National Research Council (1988), *Panel on Seismic Hazard Analysis, Committee on Seismology, Probabilistic Seismic Hazard Analysis*, 200 pp., Natl. Acad. Press, Washington, D. C.
- Wallace, L. M., J. Beavan, S. Miura, and R. McCaffrey (2009), Using Global Positioning System data to assess tectonic hazards, in *Volcanism, Tectonism*

- and *Siting of Nuclear Facilities*, edited by C. Connor, L. Connor, and N. Chapman, chap. 8, pp. 156–175, Cambridge Univ. Press, Cambridge, U.K.
- Wang, K., R. Wells, S. Mazzotti, R. D. Hyndman, and T. Sagiya (2003), A revised dislocation model of interseismic deformation of the Cascadia subduction zone, *J. Geophys. Res.*, *108*(B1), 2026, doi:10.1029/2001JB001227.
- Ward, S. N. (1998a), On the consistency of earthquake moment release and space geodetic strain rates: United States, *Geophys. J. Int.*, *134*, 172–186, doi:10.1046/j.1365-246x.1998.00556.x.
- Ward, S. N. (1998b), On the consistency of earthquake moment release and space geodetic strain rates: Europe, *Geophys. J. Int.*, *135*, 1011–1018, doi:10.1046/j.1365-246X.1998.t01-2-00658.x.
- Weichert, D. H. (1980), Estimation of the earthquake recurrence parameters from unequal observation periods for different magnitudes, *Bull. Seismol. Soc. Am.*, *70*, 1337–1346.
- Wessel, P., and W. H. F. Smith (1998), New, improved version of the Generic Mapping Tools released, *Eos Trans. AGU*, *79*, 579, doi:10.1029/98EO00426.
- Working Group on California Earthquake Probabilities (WGCEP) (1995), Seismic hazards in southern California: Probable earthquakes, 1994–2004, *Bull. Seismol. Soc. Am.*, *85*, 379–439.
- Yoshioka, S., K. Wang, and S. Mazzotti (2005), Interseismic locking of the plate interface in the northern Cascadia subduction zone inferred from inversion of GPS data, *Earth Planet. Sci. Lett.*, *231*, 239–247, doi:10.1016/j.epsl.2004.12.018.
- J. F. Cassidy, L. J. Leonard, and G. C. Rogers, Geological Survey of Canada, Natural Resources Canada, Sidney, BC V8L 4B2, Canada.
- S. Halchuk, Geological Survey of Canada, Natural Resources Canada, 7 Observatory Crescent, Ottawa, ON K1A 0Y3, Canada.
- S. Mazzotti, Geosciences Montpellier, UMR 5243, Université Montpellier 2, Place E. Bataillon, Montpellier CEDEX 5, F-34095, France. (stephane.mazzotti@gm.univ-montp2.fr)